Analysis of the Features of Reionization Cosmic Dust with DUSTiER and THESAN Simulation

Jiayi Yang*

Department of Physics, University of California, Santa Barbara, United States

*Corresponding author: jiayi_yang@ucsb.edu

Abstract. Cosmic dust presented in the universe plays an important role in light extinction and determining the metallicity of galaxies. Dust properties of galaxies closer to the Earth are easier to observe. However, the dust of more distant universes, for example, the reionization universe, is not well understood. This paper will focus on discussing attributes, distributions, and interactions of dust during the high red-shift reionization galaxies, with the aid of computer simulations. The analysis of the first introduced simulation model DUSTiER (DUST in the Epoch of Reionization) focuses on dust's mass and its extinction of UV light in reionization. The main results include observed gentle UV slope variations for stellar entities with smaller masses but considerable fluctuations for higher stellar masses. Discussion of the second model THESAN analyzes on metallicity and mass distribution of dusty galaxies. Primary results exhibit a negative relation between dust-to-metal ratio and metallicity, and an increasing dust mass share of Interstellar Stellar Medium (ISM) as the universe approaches lower redshifts. These results offer a better comprehension of dust mass during the reionization epoch and the methods used by contemporary computer models to simulate it.

Keywords: Reionization; dust; computer simulation; DUSTiER model; THESAN model.

1. Introduction

Between the stars, the vast Interstellar Medium (ISM) is the main body of heat, matter, and photon transmissions. Among them, the pattern ISM interacts with light drew particular interest as early as the 30s. Trumpler discovered in 1930 that observed photometric distances of stars deviate systematically from the actual diameter distance, growing more apparent with further stars [1]. Trumpler had altered multiple independent variables in the observation, for instance focusing only on stars in the same angular diameter. etc. but was still getting deviations. He hence deduced the existence of cosmic dust, which absorbed light. This was confirmed by Greenstein in 1938 [2], who computed the total space density of particles required for a general photographic absorption coefficient of 0.5 mag./kpc. Since then, theories of cosmic dust began to emerge. For instance, in 1946, Oort and van de Hulst proposed dust made of ice grains [3]. In the sixties, improved observatory techniques allowed for the formulation of a sophisticated silicate dust model by Hoyle and Wickramasinghe [4].

Moving to more recent times, research strongly suggests supernova (SN) to be a major source producing cosmic dust [5]. Studies on core-collapsing SN 1987A entailed interesting insights to dust formation. After the explosion, the matter of SN 1987A spread to its surrounding regions. Clumps of particles were formed, which allowed for the passage of visible and UV spectrum light. The dense clumps absorbed most of the light entering them, making it difficult to determine the actual mass of them[5]. Earliest papers even argued a mass as large as 1 solar mass [6]. The theory of clump mass ensued debate on whether SN 1987A remnants were able to gather such a large amount of dust quickly. This remained an ongoing discussion up till nowadays [7]. Besides SN, Asymptotic giant branch (AGB) stars produce large quantities of dust in their envelopes, too. Laboratory simulation provided valuable insight into this process. Experiment of Lidia Martínez et al. simulated conditions of the inner shell of a carbon-rich AGB star [8]. Their machine contained ultra-high vacuum rooms, with a nozzle ejecting carbon and hydrogen particles into the first chamber for reaction. Results were then collected in the second chamber. The simulation was conducted at a rather low temperature (close to 500 K), and an abundance of amorphous carbon nanograins and aliphatic carbon clusters were

produced, while aromatic compounds and fullerenes failed to form effectively. However, upon further heating, collected particles partially turned into aromatic species. This hinted that compounds on grain surfaces could catalyze the formation of aromatic particles in regions that heat up the grain, for example, high ultraviolet (UV) radiation regions [8].

Other than laboratory experiments, contemporary computer simulations are also great tools for better understanding cosmic dust. A recent high-resolution simulation by THESAN emphasized cosmic dust in its simulation [9-11]. THESAN reproduces the universe's evolution in the reionization period, with circumstantial depiction of dust's creation and functions. A comprehensive analysis of THESAN's result would offer interesting perspectives looking at the role dust played during the reionization. In the following sections, analysis of THESAN will be discussed in detail. A description of the reionization period would be first introduced. Following this, contemporary theories of cosmic dust in the reionization period will be presented. Features exhibited by THESAN simulation will be compared and analyzed with these theories. Actual observations' data would also be included, to demonstrate potential differences with THESAN results, and what might be causing those. In the end, this paper will discuss the limitations of THESAN, and future outlooks in this field of research.

2. Basic Description of Reionization Period

Reionization is the cosmic era during which newly formed stars emitted high-intensity Ultraviolet radiations. These radiations transmit energy into neutral hydrogen in the universe. Atomic-level collisions of photons with hydrogen atoms caused changes in their energy level. The electron broke free, leaving behind the ionized hydrogen, in other words, a single proton. This period is hence called the Reionization Epoch. The 're' in the name hints that ionization has happened before. The next section will briefly go through the cosmic history before reionization. Under the commonly accepted Big Bang model, a significant event before reionization was the recombination. During the Recombination Epoch, protons combined with free electrons, creating the first neutral hydrogen particles. The quick drop in the number of electrons led to vast numbers of photons being released. These decoupled photons formed the Cosmic Microwave Background (CMB). After the Recombination, the young universe was filled with neutral hydrogen. No radiation sources existed, and hence no light traveled through the universe. Such a period was hence often referred to as the Dark Age [12]. Fig. 1 includes an illustration of the universe after The Recombination. In the vast sea of hydrogen, regions with a slightly higher density began to pull more mass to them under gravitational force [13]. This process allowed these regions to gather more and more mass. Upon reaching enough density, high pressure inside the mass clump ignited nuclear reactions, giving birth to the first stars. These first stars were fundamentally different from the younger Population I and Population II stars that are more commonly observed today.

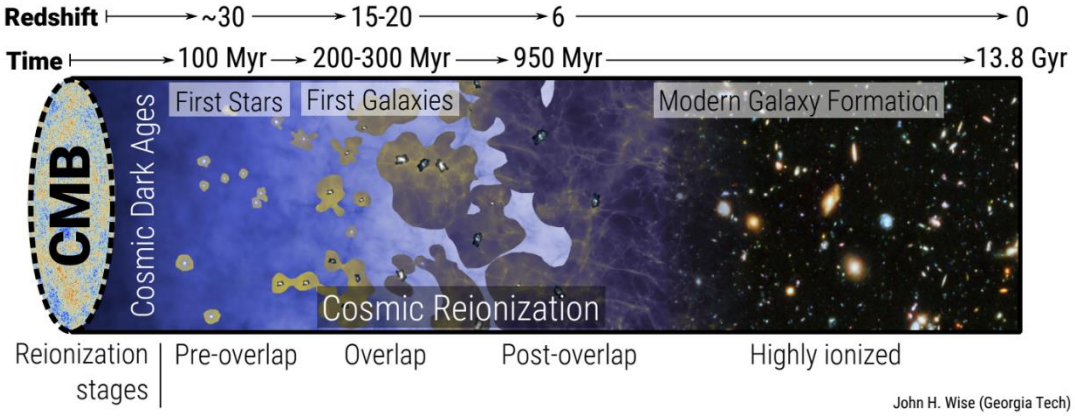

Fig. 1 The Cosmic history after The Recombination Epoch and the creation of CMB.

First stars were formed under metal-free conditions. Namely, their process of forming did not involve particles like oxygen or carbon, but only limited to hydrogen and small portions of helium.

These stars without metals were defined as Population III stars [14]. For gas to be compressed to a star, the temperature of the gas must be reduced so that its pressure decreases, and gravity force can pull groups of gas together. However, for pop III stars, without sufficient metals aiding the cooling process, alternative methods must be employed during their formation. Many mechanisms could cool the gas, but the most prominent one was radiative cooling, following atomic-level collisions [15]. As gravity force gradually compressed the gas cloud, collisions between particles became more often. Constant impacts increased the energy level of atoms. In other words, they were excited by the gain of energy. This set the stage for de-excitation to happen. As atoms fell from a high energy level back to a lower state, a photon would be released. If this photon managed to escape the compressing halo, the total energy of the halo would decrease. This prevented the gas from rising to high temperatures. Even if high temperatures were not desired during star formation since it leads to harder compression, a minimum temperature threshold was needed to be reached to cause atomic excitation. For population III stars to be able to cool, the temperature needed to be at least $10^4\ K$. For halos of mass to cool lower than this temperature, other mechanisms aiding the cooling process must be present, like metals; And this by definition made the star non-population III. With such temperature restriction, the conglomeration of mass would require a mass around $10^8_{\odot}$ [16].

Dust in the reionization period has a debated origin. Normally speaking, original dust grains come from two sources in the universe: AGB stars and Supernovas. However, due to the difficulty of observing dust in a high-redshift universe, many assumptions of contributions from these two sources are made. For different models, contributions can be vastly different, because these factors are highly unconstrained or unclear [17]. One major aim of this paper is to discuss different models of dust in the reionization high redshift galaxies, and analyze what their results tell about the dust. The first model is introduced in the following chapter.

3. DUSTiER Model

Dust in the Epoch of Reionization, or DUSTiER, is a $16cMpc^3h^{-3}$ computer simulation of 2048^3 mass cells in the model [18]. The simulation focuses on dust's formation and destruction by supernovas. This yields dust mass in each cell that can then be used to compute the reddening of light. Such computation allows DUSTiER to produce interesting results regarding Ultraviolet Luminosity Function (UVLF). The code used, methods, and results are gone over below.

weRAMSES code was first developed by Teyssier in 2001 [19]. The traditional patch-based Adaptive mesh refinement (AMR) approach drew rectangular mass units in the model. Compared to patch-based AMRs, RAMSES implements AMR with a tree-based algorithm. Resembling a "Fully Threaded Tree" [20], base elements do not take the form of singular units, but pacts of 2-dimensional sibling cells named octs. Such a structure can better compute the case when many small haloes combine to form one massive conglomeration, which would otherwise require too many grids to solve with patch-based AMR. After the construction of the base structure, the gas dynamics are calculated. An unsplit Godunov Scheme of second order is used to describe the gas on the Eulerian grid [21]. With gas dynamics computed, star formation can be then solved. The algorithm of dust models follows right next.

Each cell contains its own dust mass. To improve the efficiency of calculation, dust grains are assumed to be 0.1 μm, with standard solar chemical composition [18]. Dust creation and destruction are tracked in all cells and are going to be discussed now. The increase in the magnitude of dust mass comes from two sources in DUSTiER model. First, a fraction of one supernova explosion's remnants will condense into dust grains, increasing the total amount of dust. Second, after these dust grains are present in the model cell, the process of gradual mass accretion allows dust grains to grow in size and mass. Dust grains can be destroyed by either heat or supernova shockwaves. For thermal sputtering, destruction became more efficient at higher temperatures. For supernova shockwaves, dust destruction rate is proportional to the fraction $M_{s,100}/M_g$. Dust grains are set to be dismantled when

hit by shockwave higher than the speed of $100\ kms^{-1}$, and $M_{s,100}$ is the estimated mass hit by such speed; M_g is simply the total gas mass in the cell.

Intuitively, total mass of the cosmic dust grows with time in different redshift simulations. However, the pattern of dust growth varies quite significantly with different stellar masses. A plot of cell's stellar mass versus total mass of dust inside that shell is shown in Fig. 2 [18]. Overall, as mass of the cell gets larger, the cosmic dust from that cell grows more abundant. This is expected as higher cell mass means likely more supernova events in that shell, which leads to more dust. There is a wbound. These bounds are caused by system setup of DUSTiER. The maximum dust mass given a stellar mass is a certain number, as the dust mass to total metal mass ratio is set to be at most 0.5. The lower boundary is the dust mass produced by supernova explosions under different stellar masses. If one cell's data lands on the lower boundary, that would mean there is no mass accretion on dust grain happening, and all dust within the cell is from supernova events; None of the cells have zero grain accretion contribution. However, for cells with lower stellar masses ($< 5 \times 10^5\ M_\odot$), most data points land rather close to the lower boundary. This hints that most of the dust mass indeed comes from supernovas, and the accretion process is inefficient for these low-mass stellar systems. For higher stellar-mass cells ($> 10^7\ M_\odot$), dust mass contributions becomes significantly higher. In fact, for massive stellar systems, the dust mass inside has almost reached the maximum possible value. Not only for lower but also higher redshift simulations. This means that the model predicts a similar stellar mass vs. dust mass pattern for both older reionization-era galaxies and younger ones.

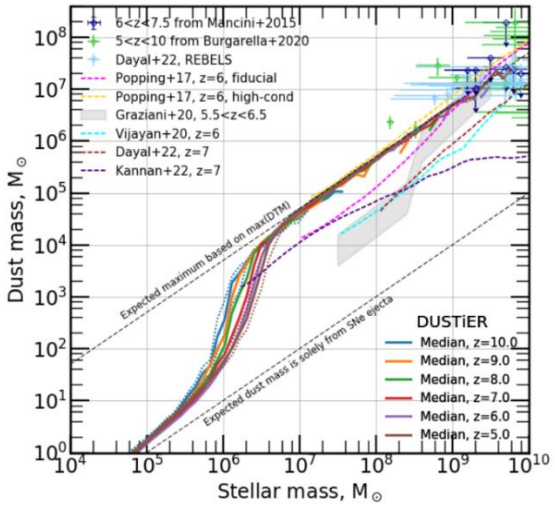

Fig. 2 Stellar mass vs. Dust mass graph under DUSTiER model, for different redshifts, with some data from other simulations referenced for comparison.

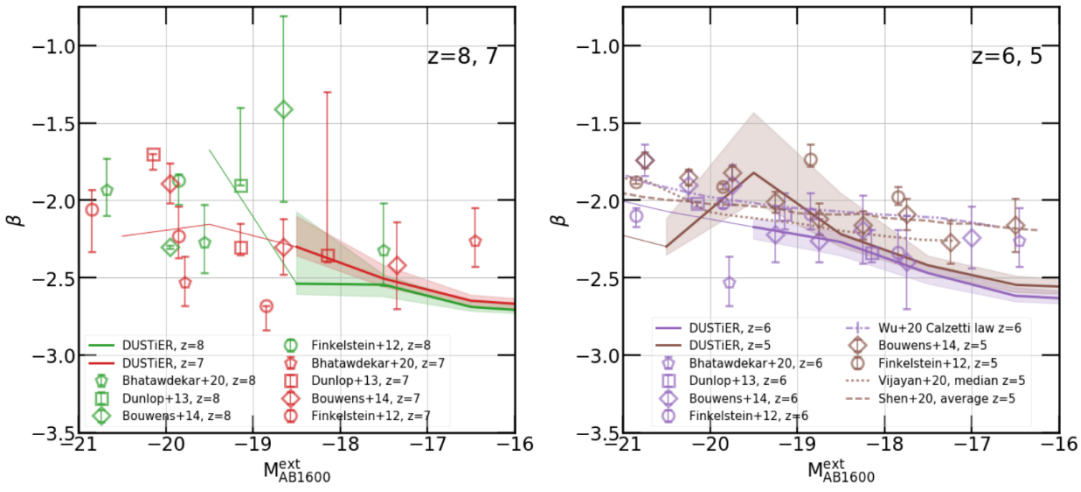

Fig. 3 The relation between β, the UV slope, and M_{AB1600}^{ext}, dust mass accounting for light extinction under redshift 8 and 7 (left) as well as redshift 6 and 5 (right).

DUSTiER focuses on the UV spectrum reddening in its model. This can be seen in its analysis of reddening around light wavelength 1600 Å. Seen from Fig. 3, M_{AB1600}^{ext} is the dust mass accounting for light reddening of 1600 Å, while β is the UV slope. As seen by the Fig. 3, brighter galaxies with more dust mass typically have higher reddening, in other words, a less steep UV slope value, than dimmer galaxies. For four redshifts values plotted, the UV slope varies by ~ 0.6 from $M_{AB1600}^{ext} = -16$ to $M_{AB1600}^{ext} = -20.5$. For galaxies with lower dust mass ($M_{AB1600}^{ext} > -16$), the curves of graph are more stable. However, higher dust mass galaxies have some significant fluctuations. For the z = 5 simulation, the UV slope increases from ~ -1.8 to ~ -2.25 then back to ~ -1.8 again. The actual value should lie between these two numbers. Such uncertainty is likely caused by the rather moderate size of DUSTiER, and actual existing differences in reddening even for same magnitude dust halos.

UV extinction in DUSTiER is implemented in the code, in order to produce results matching real observational data. In the original, non-extinct model, DUSTiER's produces results accurate only for galaxies with less massive. For example, in the z = 6 simulation, DUSTiER's outputs match observational constraints [22-24] well before M_{AB1600} reaches -18.5. As M_{AB1600} reaches more negative values, the model overshoots actual values. The outputs get drifted away even more for redshift lower than z=6. This means that the inclusion of dust is highly necessary to produce correct UV extinction levels. Thus, the extinction from cosmic dust is added to the model. Such an act indeed leads to a general drop in UVLF values, which matches the observation constraints better. This proves the importance of cosmic dust on UV extinction for reionization-level redshifts. When compared to other models, DUSTiER has a medium level on the extinction effect of UVLF. Some other model shows that the impact of extinction occurs as early as $M_{AB1600} = 17.5$ [25]. More says that extinction kicks in not until M_{AB1600} reaches around -21 [26, 27]. DUSTiER's estimation of M_{AB1600} ~ 18.5 lay in between. A non-extreme value makes the model more credible.

4. THESAN model

As mentioned in the introduction, other than supernovae explosions, dust grain growth is a big contributor to dust mass increase. A comprehensive computer simulation, THESAN model, captures characteristics of dust during reionization not only from stellar events but also grain self-growth[9]. In this chapter, dust properties from both sources in THESAN model will be discussed. An explanation of THESAN model structures and methods will be included to demonstrate the evolution of dust and its importance in the modelled reionization epoch. Two stellar events give rise to the birth of dust in THESAN model: AGB emissions and supernovae explosions. During both events, gas is released from the star to surrounding interstellar medium. A fraction of released metal is assumed to form the initial dust grains. Such fraction is dependent on two things: the type of stellar events, and carbon to oxygen ratio within the star. Once formed, dust grains can grow or be destroyed by set methods. Dust grains initially come from two possible sources: AGB or SN. After creation, dust can grow through metal accretion. The dust growth rate is modeled as follows.

$$\frac{dM_{dust}}{dt} = (1 - \frac{M_{dust}}{M_{metal}}) \frac{M_{dust}}{\tau_g} \tag{1}$$

Here, M_{metal} is the metallic gas present in a cell, while τ_g is the growth timescale. The growth time scale depends on the gas density and temperature in the cell. These settings match that of McKinnon et al. [28], a former paper by some researchers working on THESAN.

In a realistic situation, dust grains are mainly destructed in three ways: supernovae shockwaves, thermal sputtering, and atomic level collisions between dust particles. Compared to heat and shockwaves, collisions have a small contribution to the budget of dust destruction rate[29]. THESAN thus formulates the destruction rate based on shocks and heat.

$$\frac{dM_{dust}}{dt} = -\frac{M_{dust}}{\tau_{sh}} - \frac{M_{dust}}{\tau_{sp}/3} \tag{2}$$

The rate of change is contributed by τ_{sh} and τ_{sp}, shockwave and sputtering destruction timescales respectively. τ_{sh} connects cosmic dust mass with multiple attributes of shockwaves. It depends on the velocities of SN shockwaves, SN's energy, as well as the rate of SN locally. The total dust mass and efficiency of grain destruction are also coupled into the function. τ_{sp}, on the other hand, has a simpler composition than that of τ_{sh}. Since THESAN assumes that compared to sputtering of heat other non-thermal sputtering is negligible, τ_{sp} is only affected by local gas density, temperature, and the size of grain (set as 0.1 μm). This grain size is the same as that set by DUSTiER model in the former chapter, which makes both models' results more comparable.

For simulations with all redshift values, stars started with a small mass and metallicity. Then, as they grew larger in mass, metallicity began to grow too. Such a relation agrees with that of observational data [30]. A similar pattern occurs for the dust mass of a galaxy. Dust mass here is defined as the total mass of dust within two times the half-mass radius of a stellar system. As shown in Fig. 4, the log-log chart of dust mass versus stellar mass (all in terms of solar mass) within a galaxy is almost linearly increasing for $\log(M_{Star}/M_{\odot}) < 10$. A sharp drop happens at $\log(M_{Star}/M_{\odot}) \sim 10$. This might be due to the lack of data for extremely massive stars, as stellar mass with almost 10^{10} times stellar mass can hardly form in simulation. Results from another research are also presented in the chart, with significantly higher data. This might render a disagreement, but since these high data points are the upper limit of possible dust mass in its corresponding research, THESAN curves still are in reasonable agreement with it. Metals formed during stellar evolution show an interesting relation with dust. As the metallicity of a galaxy increases, the dust-to-metal ratio (DTM) decreases. Fig. 4 depicts how $\log(DTM/DTM_{MW})$ decreases monotonically as a function of $\log(Z/Z_{\odot})$ [30-33]. DTM_{MW} is the dust to metal ratio of milky way (assumed to be 0.44). $Z/Z_{\odot}$ is the metallicity of plotted star compared to that of the sun. Other researches have slightly different patterns. Popping et al., compared to THESAN, contains a profound rise of DTM around 0.6 solar metallicity [32]. This is likely due to the high rate of dust growth around high metallicities. Vijayan et al. agreed with THESAN for lower metallicities ($\log(Z/Z_{\odot}) < -0.5$), but still has a moderate rise at higher metallicities, too [33]. Interestingly, both Popping et al[32] and Vijayan et al[33] show that a rise in DTM will occur around 0.6 solar metallicity, either rather smoothly or abruptly. THESAN, however, does not include such change in its data. The reason might be that THESAN result's metallicity is capped at solar metallicity, while all other two papers include stellar entities having higher metallicity. A lack of sample data in this case can change the outcome of the pattern. THESAN can work on improving this aspect of its model in the future.

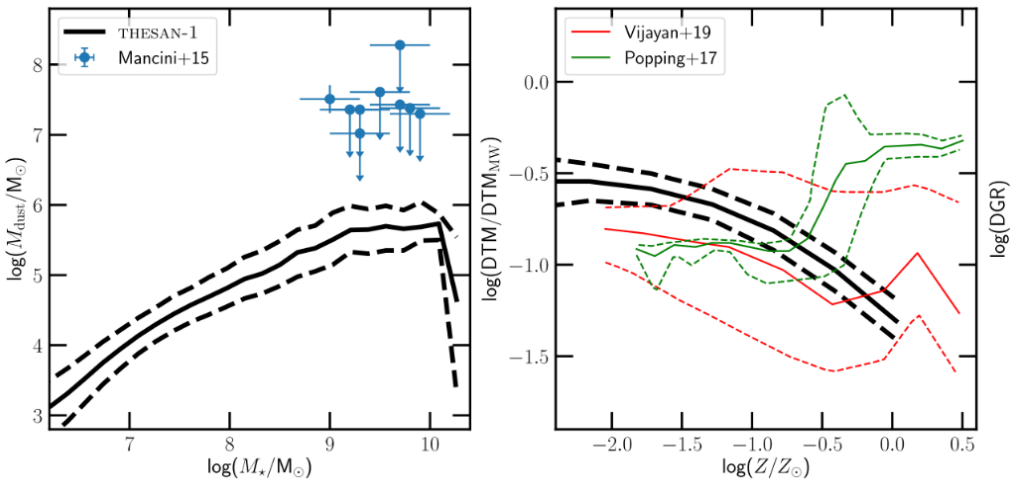

Fig. 4 Dust mass as a function of stellar mass of z=6 simulation (left) and dust to metal ratio as a function of stellar metallicity (right).

The simulated universe is divided into three regions, ISM, CGM, and IGM. Fig. 5 plots the evolution of masses throughout multiple redshifts in these regions [9]. Gas is created first in the ISM (Interstellar medium), then driven away from it by intergalactic winds of entities like blackholes.

After traveling out of the sphere with two times stellar mass radius, gas leaves the region of ISM. If gas remains in the stellar group (defined by friends-of-friends algorithm [34]), it is within the CGM region, which is the part of stellar group that is not in ISM. Any gas outside stellar groups, or in another word the mass equalling to total mass minus ISM and CGM, is in IGM (Intergalactic medium). Back to the chart, a linear relationship can be observed. As the redshift value grows, the density of both mass of metal and dust decreases. Most of dust and metal reside in CGM region. For a younger universe, Interstellar medium contains more metals than intergalactic medium. As dates go back in time, or with the increase of redshift value, Interstellar medium gradually takes less of the share and is eventually overpassed by IGM at around z=11.5. This is likely due to that in the simulated high-redshift galaxies, there are fewer stars or galactic systems than in the younger universe and the mass is more concentrated. Therefore, the size of the double half-mass-radius sphere is going to be smaller, as well as having a lesser number. These decrease the total summative volume of ISM spheres, allowing IGM to get more of the share.

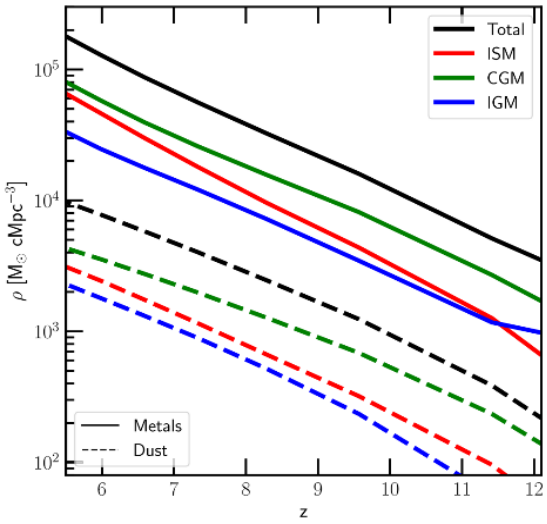

Fig. 5 Cosmic metal and dust masses as a function of redshifts.

5. Comparison and Limitations of Models

Analysis of the two model is different to showcase dust's role in the universe, during reionization. DUSTiER chapter focuses on light, while THESAN chapter analyzes on metallicity. However, this paper has included a discussion of dust mass versus stellar mass in both models, and this can be compared to indicate potential differences and what causes them. Dust mass versus stellar mass of DUSTiER in redshift z=5 to 10 is shown in Figure 2. Comparing to that of dust mass versus stellar mass graph of THESAN at z=6 in Fig. 4, DUSTiER's dust mass significantly exceed that of THESAN's. For example, for stellar mass of $10^7\ M_\odot$, THESAN has a dust mass of around $10^4\ M_\odot$, while DUSTiER has about $5 \times 10^4\ M_\odot$ dust mass not only for z=6 but also all other redshifts. At stellar mass $10^9\ M_\odot$, DUSTiER model's dust mass is $\sim 7 \times 10^6\ M_\odot$ which is more than ten times higher than THESAN dust mass at this point ($\sim 4 \times 10^5\ M_\odot$). Such big difference is likely caused by the portion of dust mass in the entire model plotted onto the graph. Specifically, THESAN is plotting dust mass only within the sphere of double stellar mass radius, or the ISM region. However, DUSTiER plots the median dust mass of the entire cell. Therefore, leading to the huge difference in mass. Another reason that might contribute to dust mass difference is that THESAN has both AGBs and supernovas producing initial dust grains in its simulations, while DUSTiER only includes that of supernovas. This is also a potential flaw of DUSTiER. As mentioned in Sec. 2, the actual attributes of dust origins (AGBs and SNs) and how they contribute remain unclear in the reionization period, and each one of them can potentially produce dust grains efficiently. In fact, there are researchers arguing that AGBs are important sources of dust grains in high red-shift reionization galaxies [35]. DUSTiER does not include any AGBs in its model.

Just like DUSTiER, THESAN has its shortcomings to be noticed too. The aspect it can improve on is already briefly mentioned earlier. THESAN has a limited number of massive stars in its simulation. Moreover, the model lacks stars that have higher metallicity than the solar metallicity. This can be a potential reason why THESAN fails to predict a rise in Dust to metal ratio for stellar entities that are metal-rich (see right panel of Fig. 4). THESAN might want to work with the inclusion of mentioned types of stars in its future improvements of the model.

6. Conclusion

To sum up, this study has introduced high-redshift reionization period's history, then presented results from two latest models DUSTiER and THESAN. They have all produced detailed computer simulations of reionization and dust in it, offering interesting perspectives. For DUSTiER, the RAMSES code of the model is introduced first, which is a tree-algorithm that improves model's performance when simulating a big number of small mass haloes. The creation and destruction of dust in the model are gone over next, with dust mass coming from a fraction of supernovae explosion and the following accretion on dust grains, which later might be destroyed by SN shockwaves. Dust mass is nearly all from supernova remnants for cells with stellar mass $< 5 \times 10^5\ M_\odot$; whereas for cells with higher stellar mass ($> 10^7\ M_\odot$), condensation of metals on dust grains becomes highly efficient, pushing dust mass to model's theoretical maximum. Focus when discussing DUSTiER is on dust' interactions with light, especially UV light. For stellar entities with lower mass, DUSTiER predicts a rather stable change in UV slope. However, for those with higher mass, dramatic fluctuations of values may come into effect, like that for z = 5 simulation. When the effect of dust on UV extinction is not counted, simulation results significantly overshoot that of observational data. After such an effect is included, DUSTiER produces curves that more accurately fit into real values.

Discussion of THESAN goes in similar structure as that for DUSTiER. Dust creation and destruction processes are presented first. Differential equations of creation and destruction in the model are presented for clarification. Then analysis of THESAN results is brought in. The main way this paper approaches THESAN's result is focusing on dust's relation to metallicity and dust distribution in the model. The log-log graphs show that as metallicity of a star rises, the dust to mass ratio around the star drops monotonically. Moreover, a linear increase in the dust mass along as a function of the stellar mass is also observed. THESAN also establishes that CGM region contains the most dust for all simulated redshifts (z = 6 to 12). Portion of dust shared by ISM gets smaller for more distant stars (higher-redshift stars in earlier reionization), and in contrast IGM's dust portion elevates. Both simulations have their limitations too. DUSTiER contains a sole analysis on supernova's production of dust grains, while THESAN does not include higher metallicity or more massive stars in the model. Nevertheless, the two models still offer valuable insights into the rather unfamiliar reionization epoch and the dust formed during it. Computer simulations, restricted by calculation potentials of current hardware and algorithms, might not be able to provide the entire picture of the universe in distant galaxies. But by starting with what is already known, models with better attributes, tuning, and resolution emerge from time to time, getting a more detailed and comprehensive picture of dust in reionization. The properties of distant galaxies hiding behind the mysterious veil will become more apparent and known in the future as simulations and observations employ more advanced tools and techniques.

References

[1] Trumpler R J. Absorption of light in the galactic system. Publications of the Astronomical Society of the Pacific, 1930, 42(248): 214-227.

[2] Greenstein J L. A determination of selective absorption based on the spectrophotometry of reddened B stars. Astrophysical Journal, vol. 87, p. 151, 1938, 87: 151.

[3] Oort J H, Van de Hulst H C. Gas and smoke in interstellar space. Bulletin of the Astronomical Institutes of the Netherlands, Vol. 10, p. 187, 1946, 10: 187.

[4] Hoyle F, Wickramasinghe N C. Interstellar grains. Nature, 1969, 223(5205): 459-462.

[5] Sarangi A, Matsuura M, Micelotta E R. Dust in supernovae and supernova remnants I: Formation scenarios. Space Science Reviews, 2018, 214: 1-48.

[6] Dwek E. Will dust black out SN 1987A. Astrophysical Journal, Part 1 (ISSN 0004-637X), vol. 329, June 15, 1988, p. 814-819., 1988, 329: 814-819.

[7] Bevan A, Barlow M J. Modelling supernova line profile asymmetries to determine ejecta dust masses: SN 1987A from days 714 to 3604. Monthly Notices of the Royal Astronomical Society, 2016, 456(2): 1269-1293.

[8] Martínez L, Santoro G, Merino P, et al. Prevalence of non-aromatic carbonaceous molecules in the inner regions of circumstellar envelopes. Nature Astronomy, 2020, 4(1): 97-105.

[9] Kannan R, Garaldi E, Smith A, et al. Introducing the thesan project: radiation-magnetohydrodynamic simulations of the epoch of reionization. Monthly Notices of the Royal Astronomical Society, 2022, 511(3): 4005-4030.

[10] Garaldi E, Kannan R, Smith A, et al. The THESAN project: properties of the intergalactic medium and its connection to reionization-era galaxies. Monthly Notices of the Royal Astronomical Society, 2022, 512(4): 4909-4933.

[11] Smith A, Kannan R, Garaldi E, et al. The thesan project: Lyman-α emission and transmission during the Epoch of Reionization. Monthly Notices of the Royal Astronomical Society, 2022, 512(3): 3243-3265.

[12] Rees M J. The universe at z> 5: When and how did the "dark age" end. Proceedings of the National Academy of Sciences, 1998, 95(1): 47-52.

[13] Wise J H. An introductory review on cosmic reionization. arXiv preprint arXiv:1907.06653, 2019.

[14] Fraser M, Casey A R, Gilmore G, et al. The mass distribution of Population III stars. Monthly Notices of the Royal Astronomical Society, 2017, 468(1): 418-425.

[15] Choudhury T R. A short introduction to reionization physics. General Relativity and Gravitation, 2022, 54(9): 102.

[16] Padmanabhan T. Theoretical astrophysics: volume 3, galaxies and cosmology. Cambridge University Press, 2000.

[17] Graziani L, Schneider R, Ginolfi M, et al. The assembly of dusty galaxies at z⩾ 4: statistical properties. Monthly Notices of the Royal Astronomical Society, 2020, 494(1): 1071-1088.

[18] Lewis J S W, Ocvirk P, Dubois Y, et al. DUSTiER (DUST in the Epoch of Reionization): dusty galaxies in cosmological radiation-hydrodynamical simulations of the Epoch of Reionization with RAMSES-CUDATON. Monthly Notices of the Royal Astronomical Society, 2023, 519(4): 5987-6007.

[19] Teyssier R. Cosmological hydrodynamics with adaptive mesh refinement-A new high resolution code called RAMSES. Astronomy & Astrophysics, 2002, 385(1): 337-364.

[20] Khokhlov A M. Fully threaded tree algorithms for adaptive refinement fluid dynamics simulations. Journal of Computational Physics, 1998, 143(2): 519-543.

[21] Fromang S, Hennebelle P, Teyssier R. A high order Godunov scheme with constrained transport and adaptive mesh refinement for astrophysical magnetohydrodynamics. Astronomy & Astrophysics, 2006, 457(2): 371-384.

[22] Bouwens R J, Illingworth G D, Oesch P A, et al. UV luminosity functions at redshifts z∼ 4 to z∼ 10: 10,000 galaxies from HST legacy fields. The Astrophysical Journal, 2015, 803(1): 34.

[23] Bouwens R J, Oesch P A, Illingworth G D, et al. The z∼ 6 Luminosity Function Fainter than− 15 mag from the Hubble Frontier Fields: The Impact of Magnification Uncertainties. The Astrophysical Journal, 2017, 843(2): 129.

[24] Livermore R C, Finkelstein S L, Lotz J M. Directly observing the galaxies likely responsible for reionization. The Astrophysical Journal, 2017, 835(2): 113.

[25] Wu X, Davé R, Tacchella S, et al. Photometric properties of reionization-epoch galaxies in the Simba simulations. Monthly Notices of the Royal Astronomical Society, 2020, 494(4): 5636-5651.

[26] Vijayan A P, Lovell C C, Wilkins S M, et al. First Light And Reionization Epoch Simulations (FLARES)--II: The photometric properties of high-redshift galaxies. Monthly Notices of the Royal Astronomical Society, 2021, 501(3): 3289-3308.

[27] Dayal P, Ferrara A, Sommovigo L, et al. The ALMA REBELS survey: the dust content of z∼ 7 Lyman break galaxies. Monthly Notices of the Royal Astronomical Society, 2022, 512(1): 989-1002.

[28] McKinnon R, Torrey P, Vogelsberger M, et al. Simulating the dust content of galaxies: successes and failures. Monthly Notices of the Royal Astronomical Society, 2017, 468(2): 1505-1521.

[29] Jones A P, Tielens A, Hollenbach D J, et al. Grain destruction in shocks in the interstellar medium. Astrophysical Journal, Part 1 (ISSN 0004-637X), vol. 433, no. 2, p. 797-810, 1994, 433: 797-810.

[30] Faisst A L, Capak P L, Davidzon I, et al. Rest-UV absorption lines as metallicity estimator: the metal content of star-forming galaxies at z∼ 5. The Astrophysical Journal, 2016, 822(1): 29.

[31] Mancini M, Schneider R, Graziani L, et al. The dust mass in z> 6 normal star-forming galaxies. Monthly Notices of the Royal Astronomical Society: Letters, 2015, 451(1): L70-L74.

[32] Popping G, Somerville R S, Galametz M. The dust content of galaxies from z= 0 to z= 9. Monthly Notices of the Royal Astronomical Society, 2017, 471(3): 3152-3185.

[33] Vijayan A P, Clay S J, Thomas P A, et al. Detailed dust modelling in the L-Galaxies semi-analytic model of galaxy formation. Monthly Notices of the Royal Astronomical Society, 2019, 489(3): 4072-4089.

[34] Springel V. The cosmological simulation code GADGET-2. Monthly notices of the royal astronomical society, 2005, 364(4): 1105-1134.

[35] Valiante R, Schneider R, Bianchi S, et al. Stellar sources of dust in the high-redshift Universe. Monthly Notices of the Royal Astronomical Society, 2009, 397(3): 1661-1671.